Desalination and Water Treatment
www.deswater.com
47 (2012) 31–41
September
1944-3994/1944-3986
doi: 10.1080/19443994.2012.696412
Taylor & Francis
Taylor & Francis Group

Adsorption of methylene blue from aqueous solutions onto sintering process red mud

Luyi Zhang[a], Huayong Zhang[a,*], Yonglan Tian[a], Zhongshan Chen[a], Lu Han[b]

[a]*Research Center for Ecological Engineering and Nonlinear Science, North China Electric Power University, Beijing 102206, China*
Tel./Fax: +86 10 80799258; email: bjecology@gmail.com
[b]*Industrial Systems Engineering, University of Regina, 3737 Wascana Parkway, Regina, Saskatchewan S4S 0A2, Canada*

Received 27 September 2011; Accepted 6 February 2012

ABSTRACT

The adsorption behavior of methylene blue (MB) dye from aqueous solutions onto sintering process red mud (SRM) and its hydrochloric acid-activated product (ASRM) was investigated in a batch system. The results showed that equilibrium was reached after a contact time of 60 min for both adsorbents. The optimum pH for MB adsorption was 10.0 for SRM and 9.0 for ASRM. The removal of the dye increased with increasing initial dye concentration and adsorbent amount, whereas it decreased with increasing ionic strength. The effect of temperature on adsorption was also investigated; the adsorption of MB on SRM and ASRM samples was spontaneous and followed an endothermic process, based on the analysis of thermodynamic parameters, including enthalpy (ΔH), entropy (ΔS), and free energy (ΔG) changes. The adsorption of MB followed pseudo-second-order kinetics, with a coefficient of correlation $\geqslant 0.9999$. The adsorption process was better described by the Langmuir isotherm model than Freundlich model, with a maximum sorption capacity of 51.7 mg/g and 61.8 mg/g for SRM and ASRM, respectively. This study demonstrates that ASRM has superior adsorbing ability for MB than SRM and can be used as an alternative adsorbent in dye removal treatment.

Keywords: Sintering process red mud; Acidification; Methylene blue; Adsorption

1. Introduction

Synthetic dyes that are widely used in textiles, coatings, paints, leather, plastics, and food have become one of the most prolific organic pollutants globally. Annually, more than 100,000 different dyes and pigments comprising 700,000 tonnes of dye are produced worldwide, and 8–12% of the unused dyes are directly discharged into streams and river [1]. These dye-containing discharges have caused various environmental problems and are hazardous to some organisms, owing to their toxic and/or carcinogenic effects, and reduce light penetration due to their color [2–4]. Thus, the treatment of the synthetic dyes from process or waste effluents is imperative for protecting the environment. However, it is rather difficult to remove these synthetic dyes from industrial waste

*Corresponding author.

wash due to their highly stable molecules and complex aromatic structures [5].

In previous years, various methods have been developed to remove dyes from effluents, including chemical coagulation and flocculation, chemical oxidation, ion exchange and neutralization, membrane filtration, adsorption, reverse osmosis, and biological treatment [6–8]. Each of these methods has inherent advantages and limitations in their applications, including high cost, low removal efficiency, and the generation of secondary pollutants. Adsorption has been found to be one of the most appealing and effective separation techniques for the treatment of dye-containing wastewater due to its low cost, simple design, and easy operation [9,10]. Activated carbon is one of the most commonly used adsorbents for dye removal due to its high surface area and large adsorption capacity [5,11]. Nevertheless, its high cost and problems that are associated with subsequent treatment and regeneration restrict its use in industrial wastewater treatment, particularly in developing countries [12]. Therefore, in recent years, many inexpensive and readily available materials such as clay materials, sepiolite, zeolites, and siliceous materials have been used to search and develop for dye removal [3,10,13,14]. In addition, some industrial and agricultural wastes such as fly ash, recycled alum sludge, red mud (RM), wheat shell, and coir pith have been also studied as potential dye adsorbents [15–18]. Utilizing industrial or agricultural solid wastes to treat dye-containing wastewaters could be helpful both to reduce costs and to solve the solid waste disposal problem.

RM, a bauxite waste of alumina manufacturing, is formed after the caustic digestion of bauxite ores during the production of alumina. Annually, approximately 90 million tonnes of RM are produced globally, and nearly 20 million tonnes of RM have been generated annually in China in recent years [19]. Due to its high alkalinity (pH 10–12.5) and large amounts, RM has had a significant environmental impact [20,21]. In previous years, some studies that applied RM in road making, land reclamation, and cement production were conducted to reuse these solid wastes [21,22]. At the same time, some researchers have also found that RM is suitable for absorbing phosphates [19,23], fluoride [24,25], arsenate [26], heavy metals [27,28], and dyes [12,20] from aqueous solution due to the nature of its constituent and its structure, which consists of a fine-grained mixture of oxides with a relatively high specific surface area [29]. However, the abovementioned studies focused on the use of Bayer process red mud (BRM), which is the primary type of solid waste generated from the aluminum industry in developed countries, and few studies investigated the utilization of sintering process red mud (SRM) or acid-activated sintering process red mud (ASRM) for the removal of dyes from aqueous solutions. In the developing countries, particularly China, RM primarily results from the sintering process of the aluminum industry due to the low grade of aluminum ore that is used [30]. Thus, a study regarding the reuse of sintering process RM in China is essential. Furthermore, due to the sintering temperature approaches 1,200˚C during the process, SRM contains active gelatin mineral components, which makes this type of RM could have potential to use as an adsorption material.

The primary objective of this work was to study the adsorption potential of methylene blue (MB) on SRM and ASRM from aqueous solutions. First, the nature and properties of SRM and ASRM were investigated. Next, the effects of contact time, pH, initial dye concentration, adsorbent dosage, ionic strength, and temperature on the properties of adsorption were evaluated. Lastly, the characteristics of adsorption isotherms, kinetics, and thermodynamics were studied.

2. Materials and methods

2.1. Preparation of the adsorbents

The samples of SRM were obtained from Shandong Aluminum Corporation in Shandong province, China. The samples were dried at 100˚C to constant weight in an air drying oven and ground to pass a 100-mesh sieve for use in subsequent experiments. ASRM was created as follows. SRM was blended with 0.5 mol/L HCl at a solid-to-liquid ratio of 1/20 in a jacketed glass reactor that was fixed in a constant temperature water bath. The mixture was then stirred for 0.5 h at 25˚C under atmospheric pressure using a digitally controlled stirrer. After stirring, the acid suspension was centrifuged for 10 min at 4,500 rpm, and then the residue was rinsed three times with distilled water to remove the residual acid. Finally, the residue was dried at 100˚C overnight and then ground to pass through a 100-mesh sieve for subsequent use.

The compositions of SRM and ASRM were determined using a Philips PW2404 X-ray fluorescence spectrometer (XRF) according to the method of GB/T14506.28-93 in China. The surface area and porous properties of the samples were determined using the Brunauer–Emmett–Teller (BET) N_2 adsorption method using the accelerated surface area and porosimetry (Quadrasorb SI, Quantachrome). X-ray diffraction (XRD) patterns of the samples were measured using a Rigaku miniflex diffractor meter with Co Kα radiation.

The microstructure and surface morphology of the samples were observed by scanning electron microscopy (SEM) using a Hitachi S-3000 N field emission scanning electron microscope. The zeta potential was determined using a Zetasizer 2000 instrument (Malvern).

2.2. Adsorbate

Analytical grade MB was obtained from Tianjin Reagent Corporation. MB is a cationic dye that contains a thiazine. The chemical formula and molecular weight of MB are $C_{16}H_{18}ClN_3SH_2O$ and 337.85 g/mol, respectively. MB has maximum absorbance at a wavelength of 664 nm in a UV–vis spectrophotometer.

2.3. Adsorption studies

MB adsorption by SRM or ASRM was measured in batch experiments. The dye solutions were prepared by dissolving a given weight of the dye in distilled water. All of the batch experiments were performed in 250-mL stoppered conical flasks containing 50 mL dye solution and shaken at 180 rpm.

The effect of contact time on adsorption was investigated by varying the contact time between MB and the adsorbents from 0 to 120 min. The initial concentration of the dye was 100 mg/L, and the adsorbent dose of the RM sample was 0.25 g/50 mL. The effect of pH was studied over a pH range of 3–10 (±0.02) with 5 g/L adsorbent at 100 mg/L dye concentration. The pH of the solution was adjusted by the addition of HCl or NaOH solutions and monitored by a pH meter (LIDA DDS-11A). The influence of adsorbent dosage was measured with varying adsorbent doses ranging from 0.05 to 0.5 g. The effect of ionic strength was investigated at 0–100 mg/L NaCl. The influence of temperature on dye adsorption was studied at 25, 35 and 45°C with 100 mg/L dye, and 0.25 g of adsorbent. For the isotherm studies, the experiments were performed by shaking 0.25 g RM samples with 50 mL aqueous solution containing various dye concentrations ranging from 10 to 500 mg/L at 25°C. At the end of each adsorption experiment, the supernatant solution was centrifuged at 4,500 rpm for 5 min. The residual dye concentration in the supernatant was analyzed by measuring the OD at 664 nm (λ_{max}) using a Shimadzu UV-2,550 UV–vis spectrophotometer. Blanks containing no dye were used for each series of experiments, and each experiment was performed in duplicate. The amount of MB that was adsorbed at equilibrium onto the adsorbent, q_e (in mg/g), was calculated by the following mass balance relationship:

$$q_e = \frac{(C_0 - C_e)V}{m} \quad (1)$$

where C_0 and C_e are the initial and equilibrium liquid phase concentrations of MB (mg/L), respectively; V is the volume of the solution (L); and m is the mass of the adsorbent that was used (g).

3. Results and discussion

3.1. Material characteristics

The compositions of SRM and ASRM as determined by XRF are shown in Table 1. The primary components in SRM and ASRM included CaO, SiO_2, Fe_2O_3, and Al_2O_3. The relative amounts of SiO_2 (24.03%) and Fe_2O_3 (20.51%) in ASRM were higher than those in SRM, whereas the content of CaO (18.22%) was lower in ASRM than in SRM (28.57%) due to the action of acid dissolving. To further illustrate the form of these elements, crystalline phases of SRM and ASRM were subjected to XRD analysis (Fig. 1). By comparing the XRD peaks between SRM and ASRM, it can be seen that the principal mineral phase of SRM was calcite, and this was followed by quartz, hematite and katoite; in ASRM, the intensity of calcite decreased, and katoite was eliminated completely. In addition, the formation of several new minerals, including magnetite and perovskite, was observed in the XRD of ASRM, which may have been due to the dissolution of the mineral phases during the acidification process.

Fig. 1 also shows the SEM pictures of SRM and ASRM. Some round-shaped aggregate particles (poorly crystallized/amorphous forms) were present in SRM, while they were become smaller and smaller aggregates were observed in ASRM. This finding indicates that some mineral phases primarily calcite that were contained in the SRM samples were dissolved in the acidic environment. This result was similar with that of the XRD experiments and suggests that the new surface area contributed to the dissolution of some of the acid soluble salts following acidification [31].

The surface area, pore volume and pore diameter of SRM and ASRM are shown in Table 1. After acid treatment, the surface area was increased to 129.5 m^2/g, which was approximately four times that of SRM. In addition, the pore volume and pore diameter were reduced from 0.460 cc/g and 100.508 nm, respectively, to 0.231 cc/g and 2.437 nm, respectively, when the sample was treated with 0.5 mol/L HCl. In addition to the changes in structure and composition, the pH of ASRM was decreased from 12.71 to 7.56. This result

Table 1
Composition and properties of SRM and ASRM

Composition	SRM	ASRM
SiO_2 (wt%)	15.93	24.03
CaO (wt%)	28.57	18.22
Al_2O_3 (wt%)	9.12	10.94
Fe_2O_3 (wt%)	13.39	20.51
MgO (wt%)	0.95	1.20
Na_2O (wt%)	3.96	0.59
K_2O (wt%)	0.40	0.13
TiO_2 (wt%)	2.58	4.13
P_2O_5 (wt%)	0.18	0.36
Others (wt%)	1.17	1.73
LOI (wt%)	23.96	18.08
pH	12.71	7.56
S_{BET} (m^2/g)	32.8	129.5
D_p (nm)	100.508	2.437
V_p (cc/g)	0.460	0.231

suggests that acidification might effectively resolve the problem of high alkalinity on RM.

3.2. Effect of contact time

A series of experiments were performed to determine the effect of contact time on the adsorption of MB by SRM and ASRM at an initial dye concentration of 100 mg/L. As shown in Fig. 2, more than 95% of MB adsorption on both adsorbents occurred within the first 10 min. After this fast initial adsorption step, the uptake rate of MB increased slowly with time, and no significant change was observed after 60 min. The concentration gradient could be responsible for these changes in MB adsorption rate relative to contact time. In the initial phase, all of the adsorbent sites were vacant, and the solute concentration was high, which led to rapid initial adsorption. As solute concentration decreased and the available adsorbed sites were reduced over time, the rate of adsorption became slower and approached equilibrium. Moreover, as seen in Fig. 2, the removal of MB was increased from 61.1 to 84.7% after acid treatment. Although acid treatment can neutralize the hydroxide ions, thereby reducing the negative charges on the surface of the RM, the surface area was enhanced considerably (Table 1). These results indicate that the adsorption of

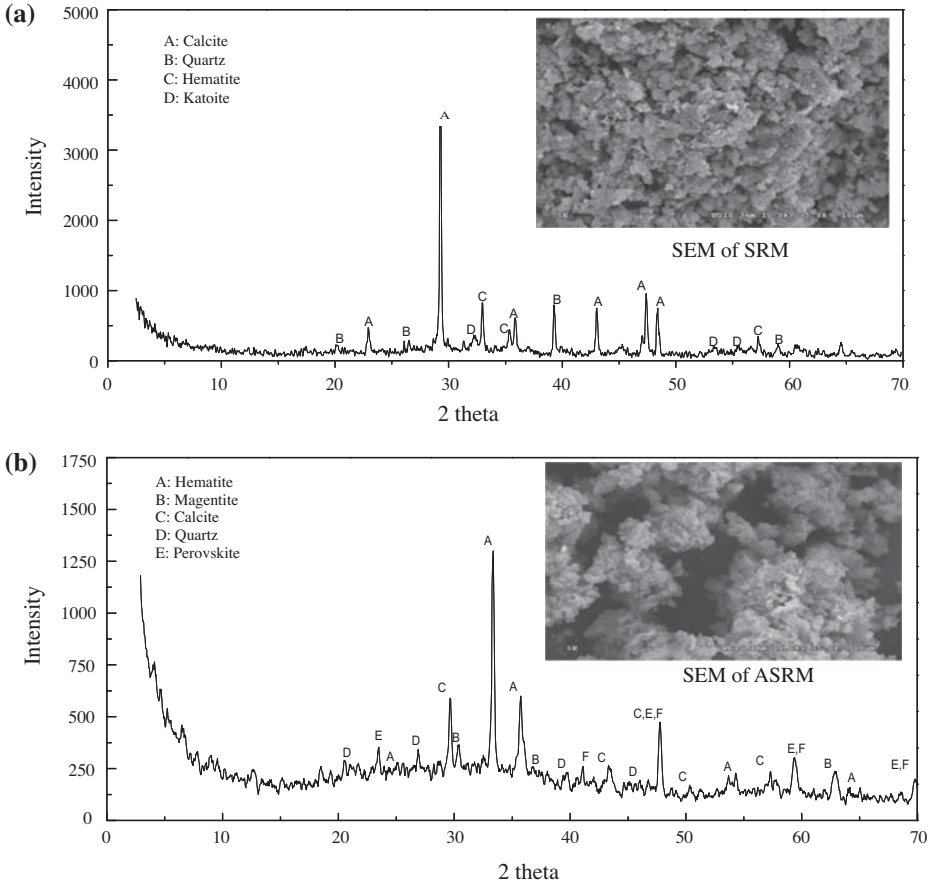

Fig. 1. The XRD and SEM photographs of SRM (a) and ASRM (b).

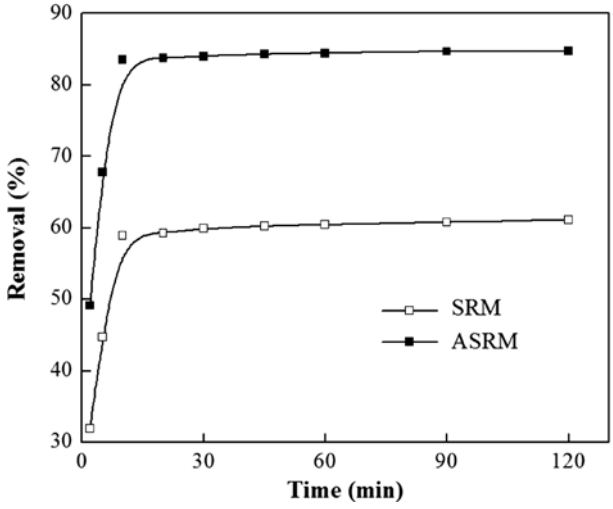

Fig. 2. The effect of contact time on MB removal by SRM and ASRM.

MB on SRM and ASRM is primarily mediated by surface physical absorption.

3.3. Effect of pH

The pH of solutions has been recognized as one of the most important factors influencing the adsorption process. The functional groups of both the adsorbent and adsorbate can be protonated or deprotonated at various pH levels and the surface charges of the adsorbent will vary with changes in pH [10]. The various uptake rates of MB onto SRM and ASRM in the pH range of 3.0–10.0 are shown in Fig. 3(a). The adsorption of MB tardily increased with increasing pH for the two adsorbents, and reached the high value when the pH value was alkalinity. Thus, alkalinity was considered as optimum pH condition for MG adsorption onto adsorbents. The maximum adsorption was 66.2% at pH 10 for SRM and 85.4% at pH 9.0 for ASRM. As the pH increased, the number of negatively charged active sites on the surface of the adsorbent increased and the number of positively charged sites decreased. Thus, the electrostatic attraction between the positive charge of MB and the negative charges on the surface of SRM and ASRM was increased, resulting in enhanced adsorption capacity. The minimum adsorption capacity of MB was found at the initial pH of 3.0 and this was likely due to the high H^+ concentration competing with the cationic groups of the dye molecule for the adsorption sites on the SRM samples. A similar trend was reported for MB adsorption on wheat shells [17] and coir pith carbon [18].

The effect of pH was also dependent on the zero point charge of the adsorbent surface (pH_{zpc}). As shown in Fig. 3(b), the zeta potential of the two adsorbents was negative (except at pH 2.0 for SRM), which indicates that negative surface charges were present on the adsorbents. Thus, as a form of cationic dye, MB dye was readily absorbed by the two adsorbents within the experiment pH range of 3.0–10.0. In addition, the highest negative was observed at pH 10.0 and 9.0 for SRM and ASRM, respectively, at which both the electrical conductivity and adsorption capacity were maximal. To compare the two materials further, neutral pH was selected for the subsequent experiments.

3.4. Effect of initial concentration

The influence of the initial concentration of MB on adsorption by SRM and ASRM was investigated at 25°C (Fig. 4(a)). Increasing the initial concentration from 10 to 500 mg/L increased the adsorption capacity

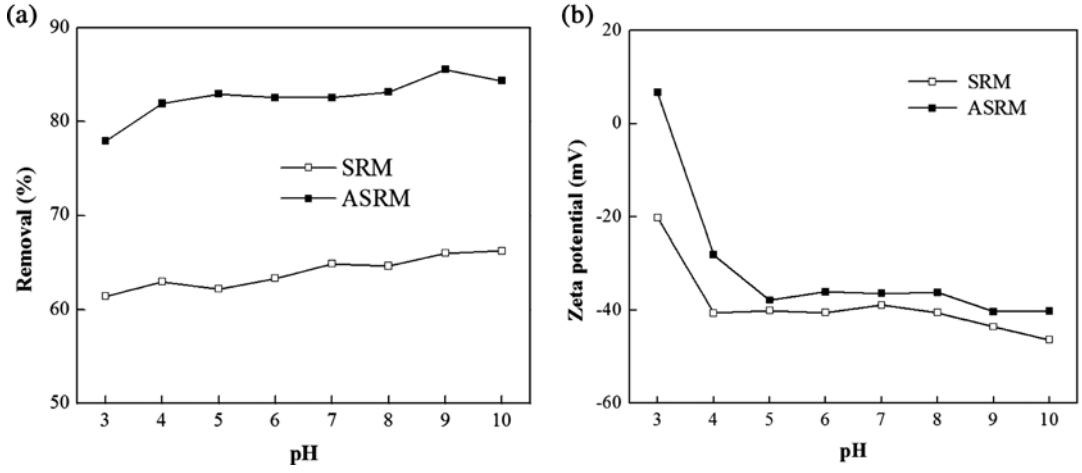

Fig. 3. The effect of initial pH on MB removal (a) and the zeta potential of the adsorbents (b).

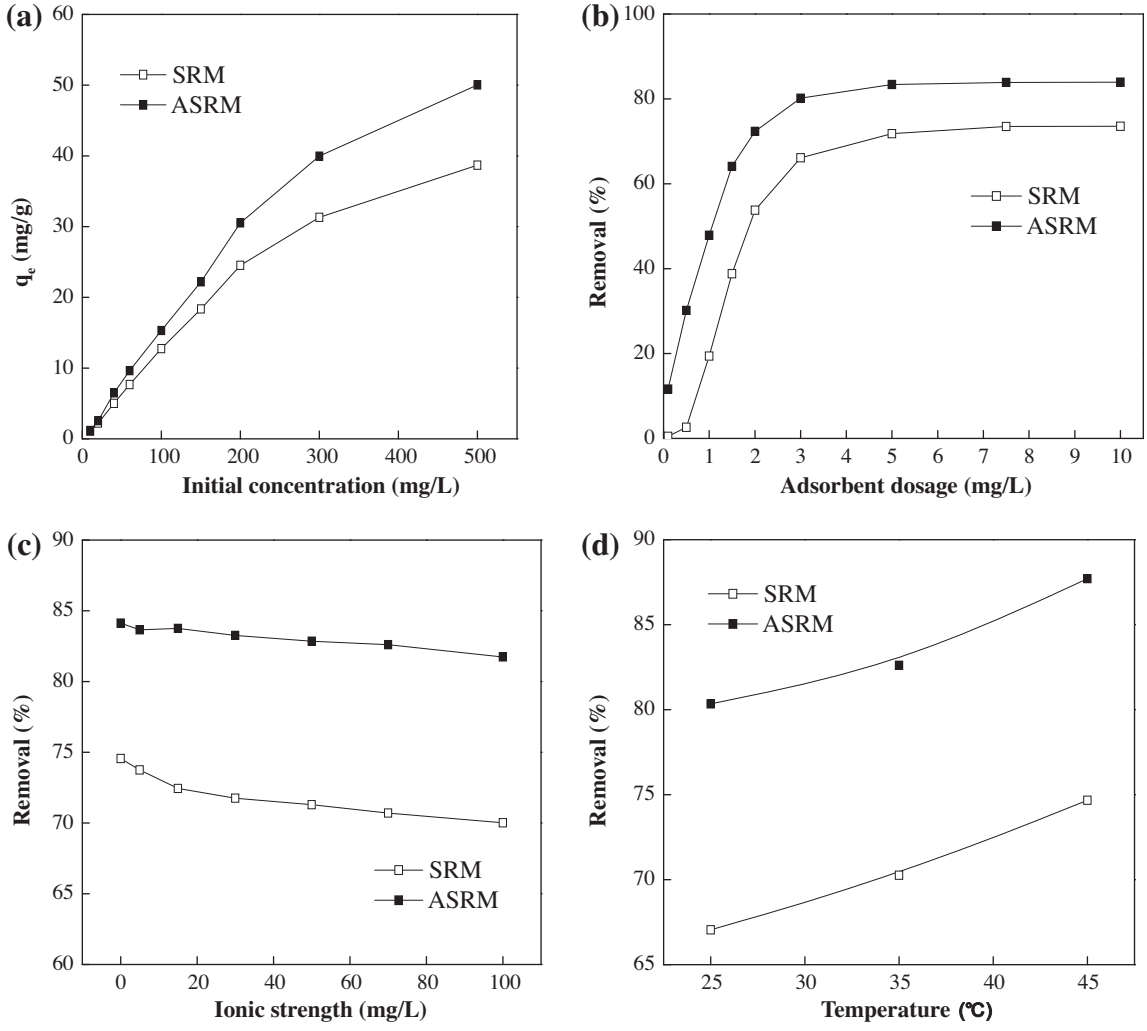

Fig. 4. The effect on the removal of MB by SRM and ASRM: (a) initial dye concentration; (b) adsorbent dosage; (c) ionic strength; and (d) temperature.

of SRM from 1.1 to 37.8 mg/g and increased the adsorption capacity of ASRM from 1.2 to 50.0 mg/g. These increases may be attributed to improved utilization of the adsorption sites and a stronger driving force of the concentration gradient at a high initial concentration. By comparing the adsorbed quantities with various initial concentrations, a linear increase in the uptake capacity of MB by both adsorbents was revealed when the dye concentration was less than 200 mg/L. This result demonstrates that the dye concentration had no effect on the adsorption mechanism below 200 mg/L [32].

3.5. Effect of adsorbent dosage

Fig. 4(b) shows the results of experiments that measured the effect of adsorbent dosage on MB removal. These experiments revealed that the removal efficiency of MB by SRM and ASRM was increased with an increase in adsorbent dosage. With an increase in the adsorbent dose from 0.1 to 10 g/L, the removal efficiency of SRM was increased from 0.5 to 73.6%, and the removal efficiency of ASRM was increased from 11.7 to 84.0%. A rapid increase in the rate of MB removal was observed at adsorbent doses between 0.1 and 5 g/L, above which a plateau in the rate of MB adsorption occurred (from 5 to 10 g/L). The fast increase in uptake with increasing adsorbent dosage may be due to the increased presence of available adsorption sites on the surface area in the range of adsorbent doses from 0.1 to 5 g/L. Above the critical dose (5 g/L), the extent of adsorption increased slowly, and this can be attributed either to the formation of aggregates at higher solid/liquid ratios or to the precipitation of particles [33].

3.6. Effect of ionic strength

In practice, various salts and metal ions are present in dye wastewater. The salts lead to high ionic strength, which may affect dye adsorption onto an adsorbent. Fig. 4(c) shows the influence of NaCl on the removal of MB by SRM and ASRM. The removal of MB by each adsorbent had a decrease with increasing NaCl concentration from 0 to 100 mg/L. The presence of NaCl in the solution may have two opposing effects. On the one hand, the salt caused a decrease in the electrostatic interaction between the opposite charges of the oxide surface and the dye molecules, which caused the removal of the dye to decrease with increasing NaCl concentration. On the other hand, with an increase in the degree of dissociation of the dye molecules by facilitating protonation, increasing the salt concentration increased the removal of the dye [12,34]. The decrease in adsorption rate with increasing ionic strength could be attributed to the competition between MB cations and Na^+ ions for the adsorption sites, and the former effect of NaCl appeared to dominate the removal of MB by the RM samples in our study.

3.7. Effect of temperature

The influence of temperature on MB by SRM and ASRM was investigated at three different temperatures (namely, 25, 35, and 45°C) at an initial MB concentration of 100 mg/L (Fig. 4(d)). With an increase in temperature from 25 to 45°C, the removal efficiency of MB by SRM increased from 67.0 to 74.7%, and the removal efficiency of MB by ASRM increased from 83.3 to 87.8%. These increases might be due to increased mobility of the dye and a higher availability of active surface sites at higher temperatures [35]. This result indicates that higher temperatures favor the removal of MB by adsorption onto SRM and ASRM. Furthermore, some thermodynamic parameters namely enthalpy change ΔH, entropy change ΔS, and free energy change ΔG were measured to study further the influence of temperature on MB adsorption. These parameters were determined based on the experimental data using the following equations:

$$K_d = \frac{q_e}{C_e} \tag{2}$$

$$\Delta G = -RT \ln K_d \tag{3}$$

$$\ln K_d = \frac{\Delta S}{R} - \frac{\Delta H}{RT} \tag{4}$$

where K_d is the distribution coefficient for adsorption (L/g), R is the gas constant (8.314 kJ/mol K^{-1}) and T is temperature (K). The values of ΔH and ΔS were calculated by the slope and intercept, respectively, of ln K against $1/T$, and the results are presented in Table 2. The values of ΔH were 14.57 kJ/mol and 22.14 kJ/mol for SRM and ASRM, respectively. These positive values confirmed the endothermic nature of the adsorption process for these two absorbents. Changing the temperature from 25 to 45°C changed the energy change, ΔG, from −1.73 to −2.82 kJ/mol for SRM and from −3.05 to −4.74 kJ/mol for ASRM. This result indicates that physical adsorption was the predominant mechanism of MB adsorption by SRM and ASRM due to the energy change of less than −20 kJ/mol [10]. In addition, the negative values in the data suggest the feasibility and spontaneous nature of the adsorption of MB. The positive values in the ΔS data suggest an increase in randomness at the interface of SRM and ASRM solutions during the adsorption process [35].

3.8. Adsorption kinetics

Kinetic models can be helpful for understanding the mechanism of adsorption and for evaluating the performance of an adsorbent. In this study, three kinetic models a pseudo-first-order model, a pseudo-second-order model, and an intraparticle diffusion model were used to test the dynamic experimental data. The pseudo-first-order model is represented by the following equation:

Table 2
Thermodynamic parameters for the adsorption of MB

Adsorbent	ΔG (kJ/mol)			ΔH (kJ/mol)	ΔS (J mol^{-1} K^{-1})
	25°C	35°C	45°C		
SRM	−1.73	−2.27	−2.82	14.57	54.67
ASRM	−3.05	−3.89	−4.74	22.14	84.50

Table 3
Comparison of the three kinetic models for MB adsorption

	Adsorbent	SRM	ASRM
Pseudo-first-order model	q_e (exp)(mg/g)	12.18	16.88
	q_e (mg/g)	3.30	2.13
	R^2	0.8281	0.7225
Pseudo-second-order model	k_2 ($g\,mg^{-1}\,min^{-1}$)	0.081	0.179
	q_e (mg/g)	12.22	16.86
	R^2	0.9999	0.9999
Intraparticle diffusion model	k_{d1} ($mg/g\,min^{1/2}$)	3.083	3.905
	C_1	1.997	4.444
	R^2	0.9999	0.9932
	k_{d2} ($mg\,g^{-1}\,min^{-1/2}$)	0.052	0.028
	C_2	11.63	16.58
	R^2	0.9482	0.9225

$$\ln(q_e - q_t) = \ln q_e - k_1 t \quad (5)$$

where q_e and q_t are the amounts of adsorbate that are adsorbed on the adsorbent (mg/g) at equilibrium and at time t, respectively, and k_1 is the constant of the pseudo-first-order adsorption (L/min) calculated from a plot of $\ln(q_e - q_t)$ vs. t. The values of q_e were not in agreement with the experiment data, and the correlation coefficients were low (< 0.9) (Table 3). Thus, the pseudo-first-order model was not suitable for describing the adsorption processes of MB on either SRM or ASRM.

The pseudo-second-order model is represented by the following equation:

$$\frac{t}{q_t} = \frac{1}{k_2 q_e^2} + \frac{t}{q_e} \quad (6)$$

where q_e and q_t are the same as in the pseudo-first-order model, and k_2 is the adsorption rate constant for this model ($g \cdot mg^{-1} \cdot min^{-1}$). Fig. 5(a) shows that the plots of t/q_t vs. t were a straight line for both SRM and ASRM. The values of q_e and k_2 were calculated from the slope and intercept, respectively, of these straight lines. The correlation coefficients of the pseudo-second-order model were value ($\geqslant 0.9999$), as shown in Table 3. The calculated equilibrium adsorption capacities, q_e, for this model were 12.22 and 16.82 mg/g for SRM and ASRM; respectively, which

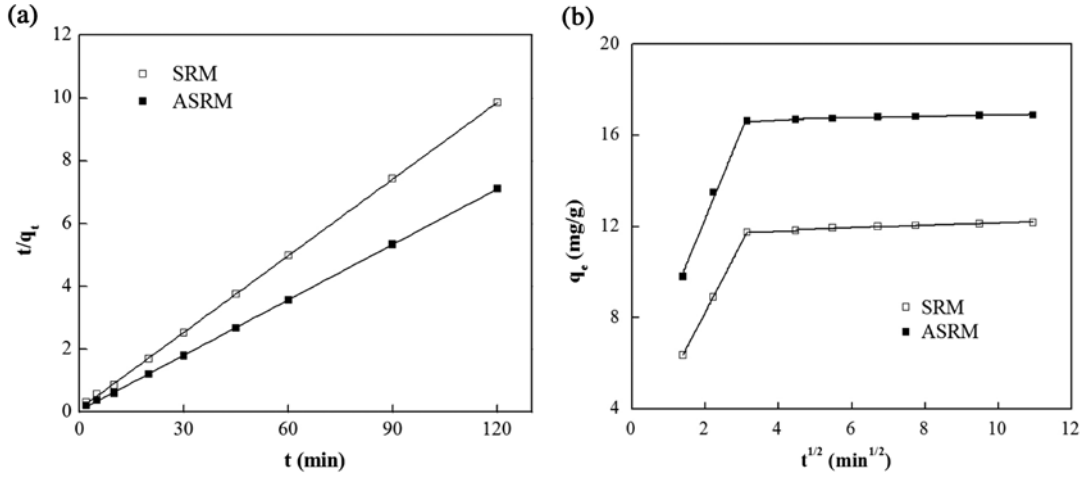

Fig. 5. Kinetic plots for MB adsorption based on (a) the pseudo-second-order model and (b) an intraparticle diffusion model.

are quite close to the experimental values (Table 3). Thus, the adsorption processes of these two absorbents were well described by the pseudo-second-order model.

To assess the rate-limiting step of MB adsorption, an intraparticle diffusion model was used. This model is represented by following equation:

$$q_t = k_d t^{0.5} + C \quad (7)$$

where k_d is the intraparticle diffusion rate constant ($mg \cdot g^{-1} \cdot min^{-1/2}$), and C is the constant relating to the thickness of the boundary layer (mg/g). Generally speaking, any adsorption process involves the following three primary, successive transport steps: film diffusion, intraparticle or pore diffusion, and sorption onto interior sites. However, the final step is considered negligible, as it occurs rapidly; hence, sorption is controlled by either film diffusion or pore diffusion, depending on which step is slower [36].

The plots of q_t vs. $t^{1/2}$ are shown in Fig. 5(b) and suggest that two different stages were exited in the adsorption process of MB onto SRM and ASRM. The sharply increasing phase within the first 10 min can be attributed to boundary layer diffusion through the instantaneous or external surface of the adsorbents. After this initial phase, a slowly increased step contributed to the transport through the pore in the SRM and ASRM by intraparticle diffusion. Other authors have reported similar kinetic results of MB adsorption on sepiolite [2] and activated carbon that was prepared from the dead leaves of *Posidonia oceanica* (L.) [8]. The intraparticle rate constants k_{d1} (for the first phase) and k_{d2} (for the second phase) were obtained from the plot of q_t vs. $t^{1/2}$ (Table 2). The values of k_{d1} were higher than for k_{d2}; thus, it can be concluded that the rate-limiting step in the present adsorption processes was intraparticle diffusion. However, neither of the intercepts passed through the origin of the coordinate axes in the plot, which indicates that intraparticle diffusion was not the sole rate-limiting step for MB adsorption onto the two absorbents.

3.9. Adsorption isotherm

The adsorption isotherm provides vital information regarding the optimum use of adsorbents in both theory and practice and describes the relationship between the mass of the substance that is adsorbed at constant temperature and its concentration in the equilibrium solution. In this study, two most commonly accepted adsorption isotherms namely, the Langmuir and Freundlich models were used to fit the experimental data for MB adsorption on SRM and ASRM at 25°C.

The Langmuir model is the simplest theoretical model for monolayer adsorption onto a surface and assumes that all of the adsorption sites have equal adsorbate affinity [17]. This model is represented by the following equation:

$$q_e = \frac{q_m b C_e}{1 + b C_e} \quad (8)$$

where C_e is the equilibrium concentration in solution (mg/L), q_e is the mass of the adsorbate per mass unit of adsorbent at equilibrium (mg/g), q_m is the Langmuir adsorption maximum (mg/g), and b is the empirical constant that is related to the binding strength of the dye (L/mg).

The characteristic parameters and the correlation coefficients (R^2) of the Langmuir model are listed in Table 4. The correlation coefficients for the two adsorbents were all higher than 0.99, which indicates that the adsorption of MB followed the Langmuir isotherm model. The maximum MB adsorption capacity was estimated to be 51.7 and 61.8 mg/g for SRM and ASRM, respectively. The Langmuir constant b was 0.0097 and 0.0159 L/mg for SRM and ASRM, respectively. The adsorption capacity can be correlated with the variations in surface area and the porosity of the adsorbent [3]. Thus, the higher surface area and pore volume in ASRM may be the primary reasons for the higher MB adsorption capacity of ASRM relative to SRM.

To determine whether the adsorption process was favorable, a dimensionless separation factor, R_L, was also measured. This factor can be calculated using the following equation:

Table 4
Adsorption isotherm constants for MB adsorption

	Langmuir model			Freundlich isotherm		
	b (L/mg)	q_m (mg/g)	R^2	K_F ($mg^{1-1/n} \cdot L^{1/n} \cdot g^{-1}$)	$1/n$	R^2
SRM	0.0097	51.7	0.9944	1.86	0.54	0.9452
ASRM	0.0159	61.8	0.9905	3.33	0.50	0.9329

$$R_L = \frac{1}{1 + bC_0} \quad (9)$$

When R_L is between 0 and 1, favorable adsorption is established. An R_L value of >1 represents unfavorable adsorption, whereas an R_L value of 1 indicates linear adsorption; if $R_L = 0$, then adsorption is irreversible [11]. At an initial MB concentration ranging from 10 to 500 mg/L, the calculated values of R_L for SRM were in the range of 0.18–0.92, and the calculated values of R_L for ASRM were in the range of 0.011–0.86. These results confirm that both adsorbents were favorable for MB adsorption. Additionally, these results demonstrate that it was monolayer adsorption on the two adsorbents and that adsorption occurred at specific homogeneous sites within the adsorbent.

The Freundlich isotherm is used for heterogeneous systems in which the heat of adsorption decreases in magnitude with an increasing extent of adsorption [18]. The Freundlich isotherm describes the ratio of the amount of solute that is adsorbed onto a given mass of adsorbent to the concentration of solute in the solution. This model is represented by the following equation:

$$q_e = K_F C_e^{1/n} \quad (10)$$

where C_e and q_e have the same meanings as described above, K_F is an empirical constant that is used to indicate the extent of the adsorption by representing the quantity of adsorption onto the adsorbent per unit equilibrium concentration, and $1/n$ is the heterogeneity factor that is considered as the parameter characterizing system heterogeneity. The Freundlich constants are calculated from the slope and intercept of $log\ q_e$ vs. $log\ C_e$. Although the correlation coefficients were larger than 0.93 (Table 4), they were still smaller than those that were obtained with the Langmuir model. This finding indicates that the Langmuir model provided a better fit than the Freundlich model for MB adsorption on SRM and ASRM. Other studies reported similar results for MB adsorption by rice husk [4] and wheat shells [17]. The values of $1/n$ were all lower than 1, which indicates high affinity between the adsorbents and MB [32].

4. Conclusions

In the present study, the potential and adsorption characteristics of SRM and its acid-activated samples (ASRM), both of which were used as adsorbents for MB removal from aqueous solutions, were investigated. Acid treatment clearly affected the removal of MB on SRM. According to the Langmuir isotherm model ($R^2 > 0.99$), the adsorption capacity of MB on ASRM was 61.8 mg/g, which was higher than the capacity of SRM (51.7 mg/g). The adsorption processes reached equilibrium at 60 min for SRM and ASRM. The adsorption rate was slowly increased with increasing pH, and the optimum pH for MB adsorption was 10.0 and 9.0 for SRM and ASRM, respectively. The initial dye concentration, adsorbent amount and temperature increased the adsorption of MB, whereas ionic strength decreased the uptake rate. The calculated thermodynamic parameters indicated that the two adsorption processes were both endothermic and spontaneous. Both of the adsorption processes were best described by pseudo-second-order kinetics and were controlled by both intraparticle diffusion and surface adsorption. This study shows that SRM materials can be considered low-cost adsorbents for the removal of MB from wastewater, with ASRM having better adsorption properties.

Acknowledgements

This work was supported by the National Water Special Project (2009ZX07210-009) and the National Science and Technology Support Project (2006BAC10B03).

References

[1] B. Noroozi, G.A. Sorial, H. Bahrami, M. Arami, Adsorption of binary mixtures of cationic dyes, Dyes Pigments 76 (2008) 784–791.
[2] M. Doğan, Y. Özdemir, M. Alkan, Adsorption kinetics and mechanism of cationic methyl violet and methylene blue dyes onto sepiolite, Dyes Pigments 75 (2007) 701–713.
[3] B.K. Nandi, A. Goswami, M.K. Purkait, Adsorption characteristics of brilliant green dye on kaolin, J. Hazard. Mater. 161 (2009) 387–395.
[4] P. Sharma, R. Kaur, C. Baskar, W.J. Chung, Removal of methylene blue from aqueous waste using rice husk and rice husk ash, Desalination 259 (2010) 249–257.
[5] E.N. El Qada, S.J. Allen, G.M. Walker, Adsorption of basic dyes from aqueous solution onto activated carbons, Chem. Eng. J. 135 (2008) 174–184.
[6] P.J. Halliday, S. Beszedits, Color removal from textile mill wastewaters, Can. Tex. J. 103 (1986) 78–84.
[7] D.T. Sponza, M. Işik, Decolorization and azo dye degradation by anaerobic/aerobic sequential process, Enzyme Microb. Technol. 31 (2002) 102–110.
[8] M. Neamtu, A. Yediler, L. Siminiceanu, M. Macoveanu, A. Kellrup, Decolorization of disperse red 354 azo dye in water by several oxidation processes-a comparative study, Dyes Pigments 60 (2004) 61–68.
[9] G. Crini, Non-conventional low-cost adsorbents for dye removal: A review, Bioresour. Technol. 97 (2006) 1061–1085.
[10] M. Alkan, Y. Doğan, Y. Turhan, Ö. Turhan, P. Demirbaş, Turan, Adsorption kinetics and mechanism of maxilon blue 5G dye on sepiolite from aqueous solutions, Chem. Eng. J. 139 (2008) 213–223.

[11] M.U. Dural, L. Cavas, S.K. Papageorgiou, F.K. Katsaros, Methylene blue adsorption on activated carbon prepared from *Posidonia oceanica* (L.) dead leaves: Kinetics and equilibrium studies, Chem. Eng. J. 168 (2011) 77–85.
[12] A. Tor, Y. Cengeloglu, Removal of congo red from aqueous solution by adsorption onto acid activated red mud, J. Hazard. Mater. B 138 (2006) 409–415.
[13] T. Sismanoglu, Y. Kismir, S. Karakus, Single and binary adsorption of reactive dyes from aqueous solutions onto clinoptilolite, J. Hazard. Mater. 184 (2010) 164–169.
[14] H.Y. Zhu, R. Jiang, L. Xiao, Adsorption of an anionic azo dye by chitosan/kaolin/γ-Fe_2O_3 composites, Appl. Clay Sci. 48 (2010) 522–526.
[15] D.S. Sun, X.D. Zhang, Y.D. Wu, X. Liu, Adsorption of anionic dyes from aqueous solution on fly ash, J. Hazard. Mater. 181 (2010) 335–342.
[16] F.A. Batzias, D.K. Sidiras, Simulation of dye adsorption by beech sawdust as affected by pH, J. Hazard. Mater. 141 (2007) 668–679.
[17] Y. Bulut, H. Aydın, A kinetics and thermodynamics study of methylene blue adsorption on wheat shells, Desalination 194 (2006) 259–267.
[18] D. Kavitha, C. Namasivayam, Experimental and kinetic studies on methylene blue adsorption by coir pith carbon, Bioresour. Technol. 98 (2007) 14–21.
[19] Y. Zhao, J. Wang, Z.K. Luan, X.J. Peng, Z. Liang, L. Shi, Removal of phosphate from aqueous solution by red mud using a factorial design, J. Hazard. Mater. 165 (2009) 1193–1199.
[20] S.B. Wang, Y. Boyjoo, A. Choueib, Z.H. Zhu, Removal of dyes from aqueous solution using fly ash and red mud, Water Res. 39 (2005) 129–138.
[21] N. Yalçın, V. Sevinç, Utilization of bauxite waste in ceramic glazes, Ceram. Int. 26 (2000) 485–493.
[22] V.M. Sglavo, S. Maurina, A. Conci, A. Salviati, G. Carturan, G. Cocco, Bauxite 'red mud' in the ceramic industry. Part 2. Production of clay-based ceramics, J. Eur. Ceram. Soc. 20 (2000) 245–252.
[23] G. Akay, B. Keskinler, A. Çakici, U. Danis, Phosphate removal from water by red mud using crossflow microfiltration, Water Res. 32 (1998) 717–726.
[24] Y. Çengeloğlu, E. Kir, M. Ersöz, Removal of fluoride from aqueous solution by using red mud, Sep. Purif. Technol. 28 (2002) 81–86.
[25] A. Tor, N. Danaoglua, G. Arslanb, Y. Cengeloglub, Removal of fluoride from water by using granular red mud: Batch and column studies, J. Hazard. Mater. 164 (2009) 271–278.
[26] H. Genç-Fuhrman, J.C. Tjell, D. McConchie, Adsorption of arsenic from water using activated neutralized red mud, Environ. Sci. Technol. 38 (2004) 2428–2434.
[27] V.K. Gupta, S. Harma, Removal of cadmium and zinc from aqueous solutions using red mud, Environ. Sci. Technol. 36 (2002) 3612–3617.
[28] A.F. Bertocchi, M. Ghiani, R. Peretti, A. Zucca, Red mud and fly ash for remediation of mine sites contaminated with As, Cd, Cu, Pb and Zn, J. Hazard. Mater. B134 (2006) 112–119.
[29] E. Kalkan, Utilization of red mud as a stabilization material for the preparation of clay liners, Eng. Geol. 87 (2006) 220–229.
[30] P.K. Zhang, Y.D. Yang, G.Q. Li, Utilization of red mud as hot metal pretreatment flux, Exp. Inf. Min. Ind. 3 (2005) 26–30.
[31] L. Santona, P. Castaldi, P. Melis, Evaluation of the interaction mechanisms between red muds and heavy metals, J. Hazard. Mater. 136 (2006) 324–329.
[32] L. Abramian, H. El-Rassy, Adsorption kinetics and thermodynamics of azo-dye Orange II onto highly porous titania aerogel, Chem. Eng. J. 150 (2009) 403–410.
[33] K. Saltalı, A. Sarı, M. Aydın, Removal of ammoniumion from aqueous solution by natural Turkish (Yıldızeli) zeolite for environmental quality, J. Hazard. Mater. 141 (2007) 258–263.
[34] N. Tekin, Ö. Demirbaş, M. Alkan, Adsorption of cationic polyacrylamide onto kaolinite, Microporous Mesoporous Mater. 85(3) (2005) 340–350.
[35] G. Moussavi, R. Khosravi, The removal of cationic dyes from aqueous solutions by adsorption onto pistachio hull waste, Chem. Eng. Res. Des. 89 (2011) 2182–2189.
[36] S.D. Faust, O.M. Aly, Adsorption Processes for Water Treatment, Butterworth, Stoneham, MA, 1987.